Interaction between Cytochrome c_2 and the Photosynthetic Reaction Center from *Rhodobacter sphaeroides*: Effects of Charge-Modifying Mutations on Binding and Electron Transfer†

M. Tetreault, S. H. Rongey, G. Feher, and M. Y. Okamura*

Physics Department, University of California, San Diego, 9500 Gilman Drive, La Jolla, California 92093

Received February 1, 2001

ABSTRACT: The electrostatic interactions governing binding and electron transfer from cytochrome c_2 (cyt c_2) to the reaction center (RC) from the photosynthetic bacteria *Rhodobacter sphaeroides* were studied by using site-directed mutagenesis to change the charges of residues on the RC surface. Charge-reversing mutations (acid → Lys) decreased the binding affinity for cyt c_2. Dissociation constants, K_D (0.3−250 μM), were largest for mutations of Asp M184 and nearby acid residues, identifying the main region for electrostatic interaction with cyt c_2. The second-order rate constants, k_2 ($1-17 \times 10^8$ M^{-1} s^{-1}), increased with increasing binding affinity (log k_2 vs log $1/K_D$ had a slope of ∼0.4), indicating a transition state structurally related to the final complex. In contrast, first-order electron transfer rates, k_e, for the bound cyt did not change significantly (<3-fold), indicating that electron tunneling pathways were unchanged by mutation. Charge-neutralizing mutations (acid → amide) showed changes in binding free energies of $\sim^1/_2$ the free energy changes due to the corresponding charge-reversing mutations, suggesting that the charges in the docked complex remain well solvated. Charge-enhancing mutations (amide → acid) produced free energy changes of the same magnitude (but opposite sign) as changes due to the charge-neutralizing mutations in the same region, indicating a diffuse electrostatic potential due to cyt c_2. A two-domain model is proposed, consisting of an electrostatic docking domain with charged surfaces separated by a water layer and a hydrophobic tunneling domain with atomic contacts that provide an efficient pathway for electron transfer.

Interprotein electron transfer plays an important role in the biological processes of photosynthesis and respiration (*1*). In these systems, water-soluble electron transfer proteins, such as *c* type cytochromes, shuttle between specific electron donor and acceptor proteins bound in intracellular membranes and carry electrons to complete intermolecular electron transfer circuits (*2*−*4*). The efficient operation of this molecular machinery requires specific binding of the electron carrier and orientation of the cofactor into a position favorable for electron transfer. In this work, electrostatic interactions important for interprotein electron transfer between the bacterial reaction center (RC) and its physiological secondary electron donor, cytochrome c_2 (cyt c_2), from the bacterium *Rhodobacter sphaeroides* were studied using site-directed mutagenesis to change the charge of the RC at the binding interface.

The RC (*5*) and cyt c_2 (*6*) proteins are key components of the photosynthetic apparatus used to convert light energy into chemical energy. The RC is a membrane protein that uses light to photo-oxidize the primary donor D, a bacteriochlorophyll dimer. The electron is transferred through a series of acceptors on the RC to a quinone Q_B, which is reduced in two successive proton-coupled one-electron steps to the quinol, Q_BH_2. The quinol dissociates from the RC, transports two electrons to reduce the cytochrome bc_1 complex, and releases two protons on the other side of the membrane. Cytochrome c_2 is reduced by the cytochrome bc_1 complex and transfers an electron to the oxidized primary donor on the RC. Thus, cytochrome c_2 acts as an electron shuttle between the RC and cytochrome bc_1, completing the electron transfer cycle that pumps protons across the membrane.

The kinetics involved in the binding and electron transfer reactions between cyt c_2 and the RC have been extensively studied by transient absorption spectroscopy using flash photolysis (*7*−*14*). Electron transfer from cytochrome c_2 to the oxidized donor is observed following photo-oxidation of the donor with a pulse of light. For isolated proteins in solution, the reaction shows at least two phases, a first-order phase ($k \sim 10^6$ s^{-1}) attributed to cyt c_2 bound to the RC and a slower phase due to the reaction of RCs with unbound cyt c_2. This reaction occurs at low ionic strength with a second-order rate constant close to the diffusion limit ($k_2 \sim 10^9$ M^{-1} s^{-1}, 10 mM). In addition, there have been earlier reports of different amounts (10−50%) of an additional first-order phase with a rate of $\sim 10^4$ s^{-1} that appears at high cytochrome concentrations (*9*, *11*, *14*). Tiede et al. found that phase to be protein preparation-dependent and attributed it to an aggregation of the RCs (*6*). Larson and Wraight have reported that slow phase artifacts may also have resulted from

† The work was supported by the NSF (Grant MCB99-74568) and NIH (Grant GM 13191).

* To whom correspondence should be addressed. E-mail: mokamura@ucsd.edu. Phone: (858) 534-2506. Fax: (858) 822-0007.

10.1021/bi010222p CCC: $20.00
Published on Web 06/27/2001

two-photon photochemistry when pulsed flash lamps were used as the excitation source (*15*). In the samples used in this study, the slow phase was not significant (less than 20% of the observed signal) and, therefore, was not taken into consideration.

The observed first- and second-order kinetics observed in isolated RCs can be described by the reaction scheme shown below (*6*).

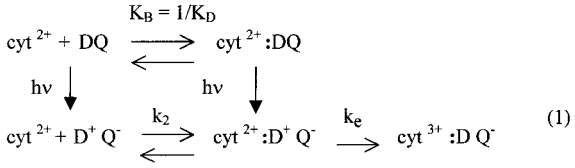

(1)

When RCs are in the neutral state (DQ) and cyt c_2 equilibrates in the dark, two populations of RCs are present, a fraction of RCs having bound cyt c_2 and a fraction with no bound cyt c_2. The fraction with bound cytochrome that displays a fast first-order rate k_e increases with increasing cytochrome concentration. Thus, the relative amplitude of the fast phase can be used to determine the dissociation constant, K_D ($=1/K_B$, the reciprocal of the binding constant), for the cyt:RC complex. The population of RC lacking a bound cytochrome must first successfully dock with cytochrome, at a rate k_2. The concentration dependence of the second phase was used to determine the rate constant k_2.

Electrostatic interactions have been shown to be important for the association of cyt c_2 and the RC. Both the second-order rate and binding affinity between cyt c_2 and the RC decrease with increasing ionic strength, consistent with the screening of electrostatic interactions (*7*, *11*, *16*). In addition, the three-dimensional crystal structures of both the RC (*17*, *18*) and cytochrome c_2 (*19*) from *Rb. sphaeroides* show regions of complementary charges that facilitate electrostatic interaction. Numerous Lys residues surround the cyt c_2 heme crevice, while many acidic residues reside on the periplasmic surface of the RC near the bacteriochlorophyll dimer. These charged residues have been shown to be involved in binding by the decreased binding affinity due to chemical modification (*20*, *21*) and site-directed mutation (*22*) of the Lys residues surrounding the heme crevice of cyt c_2 and by a preliminary study of site-directed mutation of Asp residues to Lys on the RC (*23*, *24*).

Although the importance of electrostatics for cyt c_2:RC binding is well established, the molecular details of the electrostatic interactions in forming the active complex are not well understood. To elucidate the role of these surface charges, nine Asp and Glu residues on the RC surface have been changed to Lys, Asn, or Gln residues using site-directed mutagenesis. These nine account for all but two of the negative surface charges found on the periplasmic surface of the RC. The remaining two form internal salt bridges which compensate for their charges and were therefore not considered important. Three of the mutations were located on the L subunit and five on the M subunit of the RC. Asp → Lys changes were made at the following six positions: L155, L257, L261, M88, M184, and M292. Glu → Lys changes were made at three positions: M95, M100, and M111. Four of the acids at positions M95, M184, M292, and L261 were also mutated to their neutral analogues. In addition to the changes of acidic residues, two Gln residues at positions L258 and L264 and an Asn residue at M188 were replaced with Asp or Glu residues.

The effects of the changes in charge on the binding of the cyt to the RC and on the rates of electron transfer were determined by measuring the first- and second-order electron transfer rate constants, k_e and k_2, and dissociation constants, K_D, for all the mutant RCs. These values were compared to those found in native RCs. The changes in binding due to altering charged residues on the surface were used to map out a region where strong electrostatic interactions occur in the cyt c_2:RC complex. These results, together with the relatively unchanged first-order electron transfer rates, were used to evaluate several models that had been proposed (*17*, *18*, *23*, *25*) for the structure of the complex. The second-order rate constant for electron transfer was correlated with the dissociation constant, K_D. This dependence provides information about the dynamics of the association of the functional cytochrome c_2:RC complex.

MATERIALS AND METHODS

Site-Directed Mutagenesis. Site-directed mutations were introduced into either the L (*puf*L) or M (*puf*M) genes of the RC, by using single-stranded fragments of each of these genes incorporated separately into an M13 phage. For mutants DK(L155), DK(L257), DK(L261), DN(L261), DK(M88), EK(M95), EQ(M95), EK(M100), EK(M111), DK(M184), DN(M184), DK(M292), DN(M292), and DK(L155)/DK(L257), mutations were incorporated into the AH1 or SB8 M13 vectors (*26*) using the Amersham oligonucleotide-directed mutagenesis kit. [Following the convention for naming mutants, DK(L155) represents the Asp → Lys change at position L155.] The kit protocol was followed, using synthetic 18mer oligonucleotides with the desired DNA change to introduce the mutation into the M13 vector (*27*).

For the mutants, QE(L258), QE(L264), and ND(M188) mutations were incorporated into the M13 vectors using a two-stage PCR mutagenesis protocol. A synthetic 30mer oligonucleotide containing the mutation was used as the reverse PCR primer in the reaction, while the M13/puc sequencing primer (−20) (New England Biolabs) was used as the forward PCR primer. The PCR product spanning the region between the mutation oligonucleotide to one end of *puf*L or *puf*M was then used as a megaprimer for the second reaction. The megaprimer acted as the forward PCR primer for the second reaction, while the M13/puc reverse sequencing primer (−48) (New England Biolabs) was used as the reverse PCR primer to generate the full-length product. For L subunit mutations, the PCR product was enzymatically cut with *Asp*718 and *Hin*dIII and then ligated into the M13mp19 multicloning site. For M mutations, the product was enzymatically cut with *Bam*HI and *Hin*dIII and ligated into M13mp18.

For both protocols, the L or M gene region of the single-stranded M13 mutant candidates was sequenced to confirm that only the desired mutation was incorporated. The mutated *puf*L or *puf*M DNA fragments were introduced into a pRK404-based expression vector, reconstructing the *puf* operon and creating pRKmut (*27*, *28*). The pRKmut was transferred into the *Rb. sphaeroides* deletion strain ΔLM1 via conjugation with S17 *Escherichia coli* carrying pRKmut (*29*).

Protein Expression and Purification of RCs and Cytochrome c_2. All mutant RCs were expressed in the deletion strain of *Rb. sphaeroides*, ΔLM1, which is derived from the 2.4.1 strain with the genes encoding the L and M subunits (*puf* operon) of the reaction center that had been removed. The mutant *Rb. sphaeroides* bacteria were grown aerobically as described previously (*28*). This ensured that if a mutation affected the photosynthetic viability of the bacteria there would be no bias toward revertent cells. Mutant RCs were isolated from the aerobically grown *Rb. sphaeroides* deletion strain ΔLM1 cells as described previously (*28*). The RC concentration was determined by the optical absorbance at 802 nm, using an ϵ_{802nm}^{RC} of 288 mM^{-1} cm^{-1}. Protein purity was characterized by optical absorbance ratios ($A_{280}/A_{802} \leq 1.30$).

Cytochrome c_2 was isolated from a photosynthetically grown cyt c_2 overproducing strain of *Rb. sphaeroides*, cycA1-containing copies of the plasmid pC2 P404.1 (*30*). The isolation was carried out as described previously (*31*); the cyt was ≥90% reduced. The cyt c_2 concentrations were determined from their optical absorbencies at 550 nm, using an ϵ_{550nm}(reduced) of 30.8 mM^{-1} cm^{-1} (*31*). Protein purity was characterized by optical absorbance ratios ($A_{280}/A_{417} \leq 0.25$).

Quinone/Quinol Preparations. Quinone (Q_0) (2,3-dimethoxy-5-methylbenzoquinone) was obtained from Aldrich and was >99% pure. Quinol (Q_0H_2) was formed by reducing Q_0 with hydrogen gas in the presence of platinum black (Aldrich).

Electron Transfer Measurements. Flash absorption spectroscopy was used to measure the electron transfer kinetics between cyt c_2 and the RC. The reactions were initiated by a laser pulse from either a ruby laser ($\lambda = 695$ nm, $\tau = 10$ ns) or a dye laser (Phase-R, $\lambda = 590$ nm, $\tau = 300$ ns). Absorption changes accompanying electron transfer were monitored at either 595 or 865 nm using a modified Cary 14 spectrophotometer (Varian). Flash-induced absorbance data were collected on a LeCroy oscilloscope and transferred to a computer for analysis. All measurements were performed at 23 °C in a buffer of 10 mM Hepes, 0.04% β-D-maltoside, and 0.1 mM EDTA at pH 7.5. Prior to the measurements, 0.1 mM Q_0 and 0.1 mM Q_0H_2 were added as a redox buffer, ensuring that cyt c_2 was fully reduced before each laser flash.

Measurements of the fast kinetics were taken on 10 μM samples of native and mutant RCs with cyt c_2 concentrations ranging from 5 to 300 μM. In addition to the ~1 μs signal due to the reduction of the bacteriochlorophyll dimer by cyt c_2, there was a smaller kinetic signal of unknown origin seen at 595 nm in some mutants that was not observed in the R26 RCs. When there was no cyt c_2 present, this transient ~1.5 μs signal had an amplitude ranging from 5 to 20% (depending on the mutant) of the total ΔOD^{595nm} absorbance change from photo-oxidation of the dimer after the laser flash. Experiments were carried out to determine the origin of the signal and how to resolve it from the cyt c_2 electron transfer reaction. By comparing the transient signal from native (strain 2.4.1) and mutant RCs grown both aerobically and photosynthetically, we determined that the transient signal is produced only in aerobically grown *Rb. sphaeroides*. This explains why it was not observed in the R26 strain, which was grown photosynthetically. It was established that the transient signal occurred independently of whether cyt c_2 was present during photo-oxidation and reduction of the RC. It was therefore subtracted from the absorbance signal when cyt c_2 was present to determine the correct rate of electron transfer, k_e, of the RC by cyt c_2.

The second-order rates and dissociation constants were determined on the same samples. Most mutant samples had a concentration of 1 μM. The concentration of cyt c_2 was incrementally increased as the reduction of the bacteriochlorophyll dimer by cyt c_2 was monitored at 865 nm. The fraction of RCs with cyt c_2 bound, $[RC:cyt^{2+}]/([RC] + [RC:cyt^{2+}])$, was defined as the fraction of the transient signal decaying with a rate k_e. The free cyt concentration ([cyt]) was obtained by subtracting the bound cyt concentration from the total concentration of cyt added to the sample. The dissociation constant (K_D)

$$K_D = \frac{[RC][cyt^{2+}]}{[RC:cyt^{2+}]} \quad (2)$$

for each sample was obtained by plotting the percent of cyt-bound RCs versus free cyt and fitting the results to the binding equation

$$\% \text{ bound RC} = \frac{100}{1 + \frac{K_D}{[cyt^{2+}]}} \quad (3)$$

Second-order rate constants (k_2) were determined by measuring the slow phase in the re-reduction of the RC due to the kinetics of association of cyt c_2 and the RC. The slow phase was monitored in samples where the concentration of free cyt c_2 ($[cyt^{2+}]$) was large compared to the unbound RC concentration ($[RC^+]$) so that the reaction ($d[RC^+]/dt = k_2[cyt^{2+}][RC^+]$) is pseudo-first-order. The pseudo-first-order rate, k_{obs}, was plotted verses the free cyt c_2 concentration and the second-order rate constant obtained from the slope of the plot.

$$k_{obs} = k_2[cyt^{2+}] \quad (4)$$

In mutants where $K_D < 0.3$ μM, it was necessary to determine k_2 and K_D using 0.1 μM samples of RCs since in a 1 μM sample all RCs were bound within our experimental resolution. Native RCs were assessed at both 1 and 0.1 μM.

Computational Model. The computational model used to analyze the binding free energies is based on the partitioning of the free energy for binding into several terms (*32*−*34*). The measured free energy for binding

$$\Delta G^\circ = k_B T \ln K_D \quad (5)$$

(where k_B is Boltzmann's constant and T the absolute temperature) is expressed as the sum of four terms (*34*).

$$\Delta G^\circ = \Delta G^{ES} + \Delta G^{DS} + \Delta G^{HP} + C \quad (6)$$

where ΔG^{ES} is the Coulomb interaction between charges q_i on residues on the RC and charges q_j on residues on the cyt. This can be represented in terms of a potential ψ_i at the position of residue i that is the sum of the potentials from all the charges on the cyt.

$$\Delta G^{ES} = \sum_i \sum_j \frac{q_i q_j}{\epsilon(r) r_{ij}} = \sum_i q_i \psi_i \qquad (7)$$

ΔG^{DS} is the desolvation energy due to solvent polarization by the charged groups. The desolvation energy arises as a reaction field energy similar to a Born charging energy which is proportional to q^2. As we show later, its magnitude is negligible for the case of the cyt:RC complex. ΔG^{HP} is the energy due to hydrophobic interactions. This includes the van der Waals interactions between hydrophobic residues and the entropy contribution due to water structure. C is a constant that corrects for the entropy change due to the loss in translational and rotational degrees of freedom due to binding and the entropy change due to dilution (cratic term). A C value of 0.40 eV (9 kcal/mol) is commonly used (*34*).

RESULTS

Electron Transfer Kinetics. Representative measurements of electron transfer kinetics between cyt c_2 and native and mutant RCs are shown in Figure 1. Following the laser pulse, the absorption at 865 nm in native RCs decreases upon oxidation of the bacteriochlorophyll dimer ($D \rightarrow D^+$). In the absence of cyt c_2, the D^+ state does not recover on the millisecond time scale, but shows charge recombination kinetics on the time scale of 0.1−1.0 s (*35*). However, in the presence of added cyt c_2, D^+ recovers faster, i.e., it is reduced, due to electron transfer from cyt c_2. The D^+ recovery has two phases: a fast phase with a rate that is independent of the cyt c_2 concentration and a slow phase with a rate that is dependent on the cyt c_2 concentration. The amplitude of the fast phase relative to the slow phase increases with increasing cyt c_2 concentrations. In native RCs, the two phases are equal when the free cyt c_2 concentration is ~0.3 μM (=K_D). In the mutant RCs, the kinetics are significantly different from those in native RCs. A representative example is shown in Figure 1b for the DK(M292) mutant. The amount of cyt c_2 required to obtain equal amplitudes of the fast and slow phases is increased (K_D = 11 μM), and the second-order rate constant obtained from the slow phase (eq 4) is decreased from 17×10^8 to 5.3×10^8 M^{-1} s^{-1}.

First-Order Electron Transfer Rates. Representative fast electron transfer kinetics for native and DK(M292) mutant RCs monitored at 595 nm are shown in Figure 2. Native RCs showed a 1 μs fast phase of D^+ reduction upon addition of cyt (Figure 2a). This rate did not depend on the concentration of cyt and is attributed to the electron transfer from bound cyt c_2. In mutant RCs, the D^+ reduction due to cyt addition also displayed a rate that was similar to that observed in native RCs (Figure 2b). The first-order electron transfer times ($\tau_e = 1/k_e$) for the mutant RCs are shown in Table 1. In contrast to the dissociation constants, none of the first-order rates of the mutants differed very much from those observed in native RCs (τ_e = 0.8 μs). The largest difference (a factor of 2−3) was seen in mutants DK(M88) and DK(M95) where the measured rates were 0.3 and 0.4 μs, respectively, and for QE(L258) where the rate was 2 μs. In some mutants, an additional transient kinetic signal was observed at 595 nm which was subtracted (see the discussion in Materials and Methods).

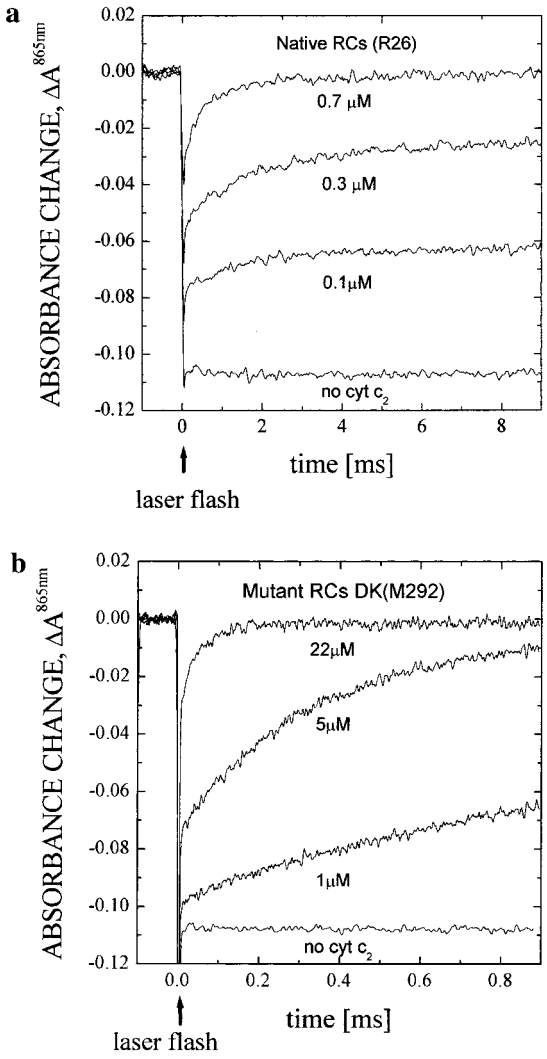

FIGURE 1: Kinetic assay of cyt c_2−RC binding and electron transfer following a saturating laser flash. The reduction of the oxidized donor by reduced cyt c_2 is monitored at 865 nm. (a) In native RCs, a fast phase indicative of electron transfer from bound cyt and a slow phase due to second-order electron transfer from free cyt are observed. (b) In mutant DK(M292) RCs, similar biphasic kinetics are observed. However, the cyt concentrations needed to observe a 50% fast phase (K_D) is much higher, and the second-order rate constant k_2 calculated from the slow phase is smaller. The RC concentration is 1 μM, and the free cyt concentrations are as shown. Buffer (pH 7.5): 10 mM Hepes, 0.04% dodecyl β-maltoside, and 0.1 mM EDTA. T = 23 °C.

Dissociation Constants. Plots of the fraction of the fast phase versus the free cyt concentration were used to obtain values for K_D using eq 3 (see Figure 3). A reasonably good fit to this equation were obtained by assuming 100% active RCs. At high occupancy (>80%), the binding curves deviated from these plots, indicating a small fraction of RCs with weaker binding. This fraction was not taken into account in determining K_D. The weak binding fraction may be due to heterogeneity in the RCs (*6*). The dissociation constants measured in native and mutant RCs span 4 orders of magnitude. They are grouped in Table 1 according to the changes in charge and are listed in order of increasing binding affinity (decreasing K_D). The change in K_D varied greatly with the position of the mutation on the RC surface.

Mutants that removed negative charge from the RC surface ($\Delta q > 0$) generally increased K_D (see Table 1). The first

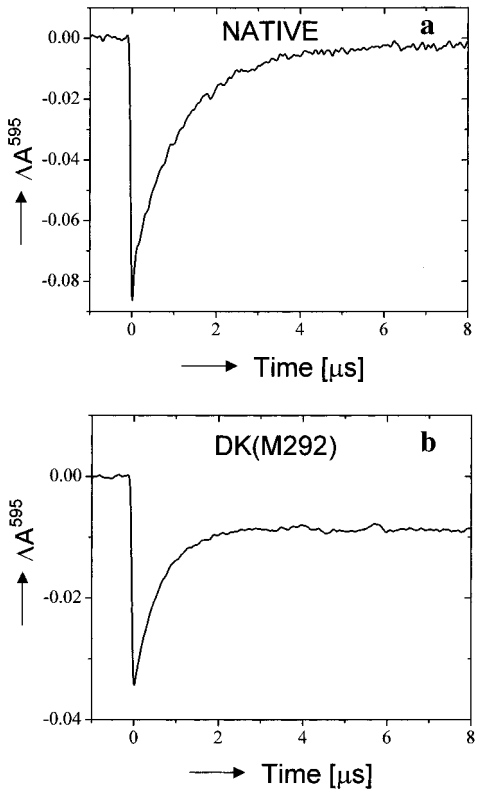

FIGURE 2: Fast phase kinetics of reduction of the oxidized donor by bound cyt in (a) native and (b) DK(M292) mutant RCs. The fast phases in native and mutant RCs are the same, in contrast to the differences in the slow phases shown in Figure 1. The pedestal in panel b is due to lack of saturation of binding. The RC concentration is 4 μM. Buffer (pH 7.5): 10 mM Hepes, 0.04% dodecyl β-maltoside, and 0.1 mM EDTA. $T = 23$ °C. The cyt c_2 concentration is 50 μM.

Table 1: Parameters Characterizing the Interactions of Cyt c_2 with Native and Mutant RCs (pH 7.5)[a]

strain	K_D[b] (μ M)	$\delta\Delta G°$[c] (meV)	τ_e[d] (μs)	k_2[e] ($\times 10^8$ M^{-1} s^{-1})	Δq
native	0.3	0	0.8 ± 0.1	17	0
DK(M184)	250	168	0.8 ± 0.2	1	2
DK(L261)	55	130	0.6 ± 0.3	3.5	2
DK(M88)	55	130	0.3 ± 0.2	2	2
EK(M95)	50	128	0.4 ± 0.2	2	2
DK(M292)	11	90	0.8 ± 0.2	5.3	2
DK(L257)	7	79	0.9 ± 0.1	7	2
DK(L155)	5.2	71	0.9 ± 0.1	7	2
EK(M100)	0.5	13	0.7 ± 0.1	8	2
EK(M111)	0.4	7	0.8 ± 0.1	10.5	2
DK(L155)/DK(L257)	100	145	1.0 ± 0.4	4	4
DN(M184)	8.4	83	0.8 ± 0.1	6	1
EQ(M95)	5	70	0.6 ± 0.2	7	1
DN(M292)	1.6	42	0.9 ± 0.1	10	1
DN(L261)	1.4	39	0.9 ± 0.1	14	1
QE(L258)	0.2	−10	2 ± 0.5	22	−1
ND(M188)	0.06	−40	1 ± 0.2	25	−1
QE(L264)	0.01	−85	0.7 ± 0.1	30	−1

[a] Mutations produce changes in charge ($\Delta q = 4$, 2, 1, and −1) as shown. [b] K_D is the dissociation constant for the RC:cyt c_2 complex. [c] $\delta\Delta G°$ [$=kT \ln(K_D^{mutant}/K_D^{native})$] is the difference in the binding free energy between mutant and native RCs. The experimental error is ±15%, unless otherwise stated. [d] τ_e is the time constant for the fast, first-order electron transfer phase. [e] k_2 is the second-order rate constant.

group contains mutations of Asp/Glu → Lys that change the charge by 2. Mutant DK(M184) exhibited the largest change in binding with a K_D that was approximately 800 times that

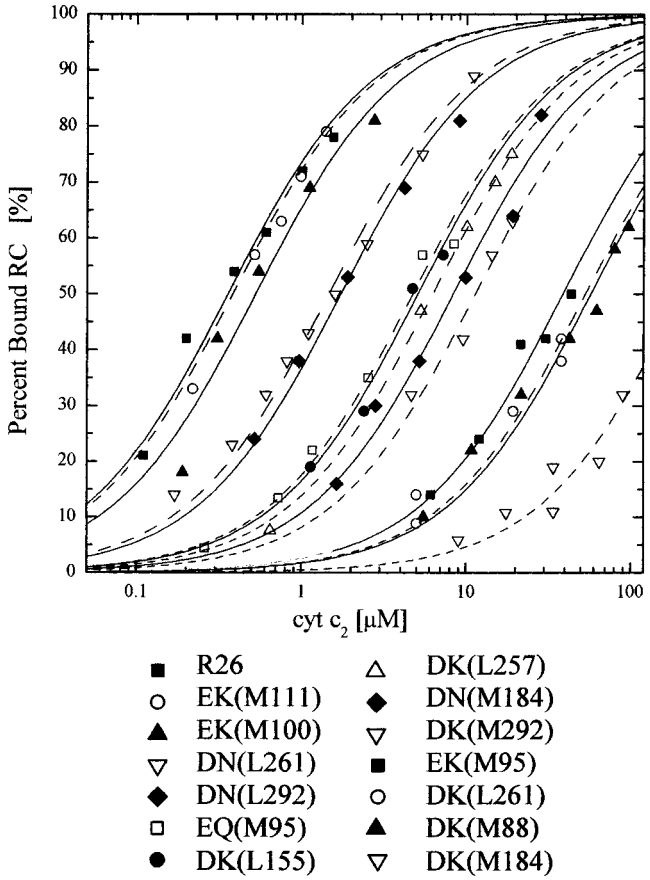

FIGURE 3: Binding curves for native and mutant RCs. The plot shows the fraction of bound cyt (the fraction of fast phase electron transfer) as a function of the concentration of free cyt. Solid and dashed lines represent fits to eq 3 with K_D as a free parameter (see Table 1). Conditions as described in the legend of Figure 1.

of native reaction centers. Three more mutants, DK(M88), EK(M95), and DK(L261), had weaker binding by a factor of ~150. Three mutants had weaker binding to a slightly lesser degree (~10−40-fold): DK(L155), DK(L257), and DK(M292). Two mutations had no significant effect on binding [EK(M100) and EK(M111)]. The double mutant DK(L155)/DK(L257), which resulted in the change in charge of 4, exhibited the second largest K_D. The four mutations in which a negative residue was replaced with a neutral residue ($\Delta q = 1$) exhibited an increase in K_D that was less pronounced than that observed in the $\Delta q = 4$ and 2 mutations.

The three mutant RCs where a neutral residue was replaced with a negatively charged residue ($\Delta q = -1$) exhibited a stronger binding of cyt. The ND(M188) and QE(L264) mutations improved binding to a significant degree (by factors of 5 and 30, respectively), whereas the QE(L258) mutation had only a small effect on binding.

Second-Order Electron Transfer Rates. The second-order rate constants were obtained by plotting the rate of the slow phase versus the free cyt concentration (see Figure 4). From the slopes of the plots k_2 was obtained (eq 4). Changes in the second-order rate constants were smaller than the corresponding changes in the dissociation constant for all mutants. The mutant DK(M184) that had the largest effect on binding, with an 800-fold increase in K_D, also had the largest effect on the second-order rate constant, with a 17-

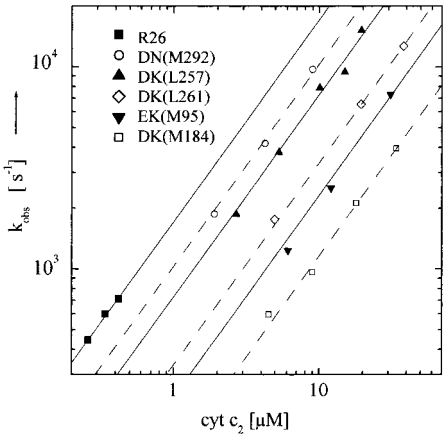

FIGURE 4: Determination of the second-order rate constants, k_2, in native and mutant RCs. The plot shows the dependence of the slow phase of electron transfer, k_{obs}, on the free cyt c_2 concentration. Solid and dashed lines represent fits to eq 4 with k_2 as a free parameter (see Table 1). Conditions as described in the legend of Figure 1.

fold decrease in k_2. For the three mutants with improved binding affinity (decreased K_D), the second-order rate constant increased. The rate constant was highest for the mutant QE(L264) with an increase of 75%. Since the binding was so strong for this mutant ($K_D = 0.01$ μM), it was necessary to measure the second-order rate at higher ionic strengths ($I = 94-220$ mM) and extrapolate back to $I = 10$ mM using the Debye−Hückel limiting law relating the rate to the ionic strength [log $k_2 \sim I^{1/2}$ (*7*)].

DISCUSSION

In this work, the effects of mutating RC surface residues on the reactions between the RC and cyt c_2 were studied. The results were used to address three major problems: (1) the structure of the cyt c_2:RC complex, (2) the role of the charged residues in the binding of the cyt, and (3) the dynamics of the association of cyt c_2 and the RC.

Structure of the cyt c_2:RC Complex

Mapping of the Docking Region from the Effect of Mutations on Binding. Since electrostatic interactions have been proposed to make an important contribution to cyt binding (*18*, *21*, *33*), mutations that change the charge on residues at the interface region can provide information about the structure of the cyt:RC complex. The spatial distribution of the changes in the cyt c_2 dissociation constant (K_D) produced by the acid → Lys mutations is displayed in Figure 5a. The periplasmic surface of the RC is shown with the bacteriochlorophyll dimer directly in the center. The binding free energy change, $\delta\Delta G°$ (see Table 1), for each mutant RC where Lys replaced an acidic residue is represented by a circle whose diameter is proportional to the change in binding free energy. This map indicates that the most significant free energy changes occur in the region of the RC near M184, L261, M95, and M88. This region is asymmetrically positioned with respect to the bacteriochlorophyll dimer. The largest interaction occurs at M184 in the center of the cluster of residues. The two residues that exhibited the smallest changes in binding, at positions M100 and M111, are located at the edge of the periplasmic surface farthest from the bacteriochlorophyll dimer. The residue at L155 located on the L side of the periplasmic surface has a relatively small effect on binding compared to M184 despite their symmetrical locations relative to the dimer. This indicates an asymmetry in cyt binding interactions.

The electrostatic contribution to the change in the binding free energy, $\delta\Delta G_i°$ (associated with the mutation of residue i), is proportional to the potential ψ_i (eq 7) due to the charges on the cyt, at the position of the charge of the mutated residue. Thus, the pattern of free energy changes shown by

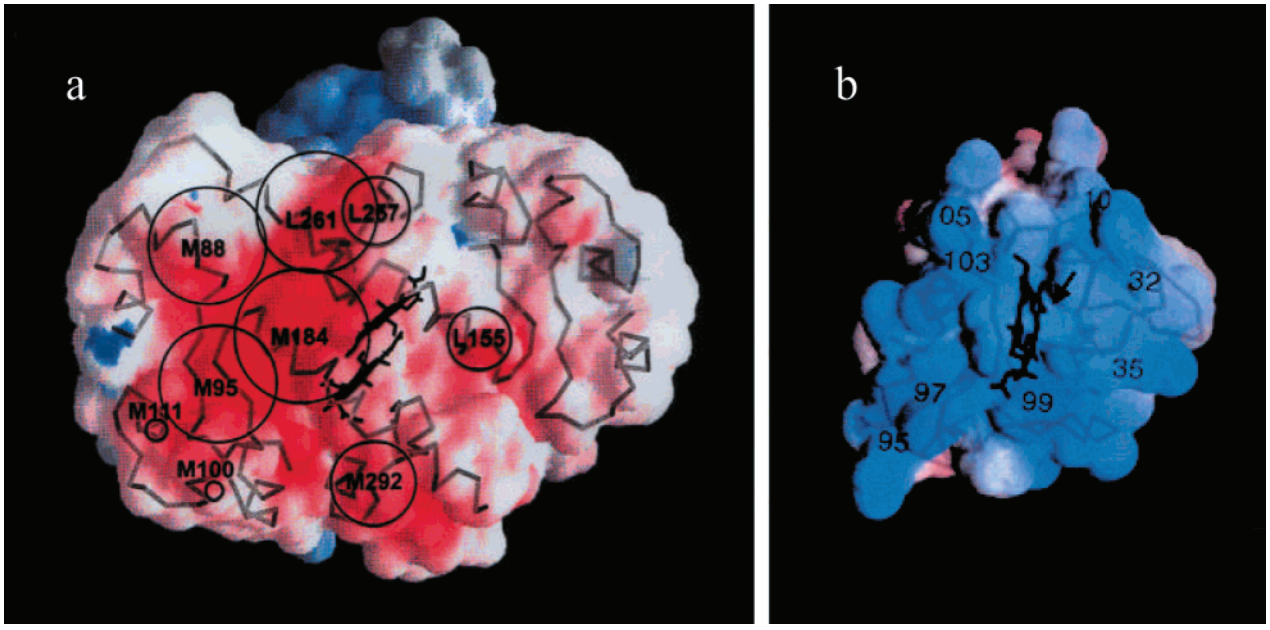

FIGURE 5: (a) Spatial distribution of free energy changes due to mutations superimposed on the electrostatic potential at the surface of the RC. The diameters of the circles around mutated residues are proportional to the free energy changes, $\delta\Delta G°$ (see Table 1), due to mutation from Asp to Lys. The potential, obtained by the Grasp program (*30*), is at the accessible surface (1.5 Å above the molecular surface). Red and blue indicate negative and positive potentials, respectively. The largest circles coincide with the region of negative potential localized on the M side of the periplasmic surface. (b) The electrostatic potential surface for cyt c_2 as seen from the docking surface. A large region of positive potential due to Lys residues is located around the exposed heme edge (arrow).

the radii of the circles at the positions of the mutated residues reflects the potential due to the cyt charges on the surface of the RC. These interactions are compared to the electrostatic potential at the RC surface obtained using the program Grasp (*36*) in Figure 5a. The red regions indicate negative potential, the blue regions positive potential. The large interaction at M184 coincides with the most negative potential region on the RC surface. The large negative potential at this site is due to contributions from Asp M184 and neighboring negative charges. In addition, Asp M184 is located in a depression on the RC surface. The surrounding low-dielectric region of the protein increases the strength of the electrostatic potential by reducing the extent of dielectric screening of the solution.

The potential map on the docking surface of the cyt c_2 from *Rb. sphaeroides* that gives rise to the interaction is shown in Figure 5b. In this view, the exposed heme edge (labeled with the arrow) is at the center. The predominantly positively charged groups surrounding the exposed heme edge (Lys 35, 88, 95, 97, 99, 103, and 105 and Arg 32) provide a strong positive potential surface that can interact strongly with the RC. Thus, the positive potential surface of the cyt and the negative potential surface of the RC form a natural docking surface.

Although the exact position of the docked complex cannot be determined from these results, it is possible to give a general picture of the most likely structure of the cyt:RC complex by overlaying the region of the cyt with large positive potential (Figure 5b) on top of the region on the RC having the largest changes due to mutation (Figure 5a). The results presented here indicate that in the complex, the region containing cyt residues Lys 95−Lys 103 are in close proximity to RC residues Asp M88, Asp M184, Asp L257, and Asp L261. This interaction has been previously proposed by several workers (*18*, *21*, *33*). An important question that needs to be answered is whether the structure of the mutant cyt:RC complex is the same as that of the native cyt:RC complex. We believe that they are the same as discussed in the next section.

First-Order Electron Transfer Rates. The first-order electron transfer rate is attributed to the rate of electron transfer from cyt c_2 to the RC in the bound state. This rate depends on both the distance between the donor and acceptor molecules and the free energy difference (driving force) for electron transfer (*37*). Preliminary measurements have shown that the redox potential of D/D^+ in the mutants DK(M184) and DK(L155) increased by only 14 mV (S. Rongey and W. W. Parson, unpublished observations). The small change in redox potential due to mutation can be explained by the solvation of the charged residues which shields them from the cofactors in the proteins. The small (14 meV) change in the driving force would increase the electron transfer rate by only 30%, according to Marcus theory, using a λ of 0.96 eV (*38*). Changes in the redox potential of the cytochrome due to mutations on the RC would be expected to be smaller in magnitude than those of the donor because of the intervening solvation layer. In addition, the effects of the mutation on the redox potentials of the cyt and donor would have opposite effects on the rate of electron transfer and would tend to cancel out if the charge changes were approximately equidistant from the two cofactors. Thus, the changes in driving force are expected to be small and have therefore little effect on the electron transfer rate. Assuming that the change in driving force due to the mutation is negligible, we can estimate the change in the distance, Δr, between the heme edge and the bacteriochlorophyll dimer upon mutation. In proteins, the electron transfer rate has been shown to decay exponentially with distance as $\exp(-\beta r)$, where r is the distance between the donor and acceptor molecules. Typical values for β have been found to be $\approx$1.4 $Å^{-1}$ (*39*). The electron transfer rate in the majority of the mutants does not change by more than $\sim$20% (see Table 1). For $\beta = 1.4$ Å, this corresponds to a distance variation Δr of $\approx$0.13 Å. In the rather exceptional case of the DK(M88) mutant, the rate changes by a factor of $\sim$3, which corresponds to a Δr of $\approx$0.8 Å. This shows that the mutations do not significantly change the distance in the cytochrome−RC complex between the heme of the cytochrome and the bacteriochlorophyll dimer (*39*, *40*).

Comparisons with Previously Proposed Structural Models. The structural predictions based on site-directed mutagenesis in the study presented here are compared in this section with previously suggested structural models for the cyt c_2:RC complex. The model proposed by Allen et al., using the three-dimensional crystal structure of the RC from *Rb. sphaeroides* and the cyt c_2 from *Rhodospirillum rubrum* (*17*), has the heme edge of the cyt centrally positioned over the bacteriochlorophyll dimer making contact with Tyr L162, similar to the structure of the cyt found in the RC from *Rhdodpseudomonas viridis* (*41*). Strong electrostatic contacts were made by rotating the cytochome so that Asp M184 is positioned near Lys 94 from cyt c_2 (equivalent to Lys 103 in *Rb. sphaeroides*; see Figure 5a,b).

In the model of Tiede and Chang, based on optical dichroism measurements, X-ray diffraction data, and electrostatic modeling (*18*), the cytochrome was shifted off center to bind more strongly to the region of negative charge on the RC surface surrounding Asp M184 (see Figure 5a). In their model, Asp M184 on the RC was proposed to interact with Lys 99 on the cyt c_2 (see Figure 5a,b).

In the model of Adir et al. (*23*), based on low-resolution X-ray diffraction data obtained on a cyt−RC cocrystal, electrostatic modeling, and a few site-directed mutations, the cyt was shifted more asymmetrically toward the M side of the RC. In this model, the heme edge of the cytochrome was positioned over Asp M184 (see Figure 5a,b).

The most recent model of Axelrod et al. (*25*) is based on improved X-ray diffraction results with cyt:RC cocrystals. In the new structure, the exposed heme edge is located over Tyr L162 in a favorable position for electron transfer, as it is in the *Rps. viridis* structure and as proposed by Allen et al. (*17*). With the current state of the refinement of the X-ray data, not all amino acid residues of the cyt are completely resolved. However, the preliminary indication is that Asp M184 is positioned close ($\sim$5 Å) to Lys 103 on cyt c_2 but not within ion-pairing distance (H. Axelrod, unpublished).

The invariance of the first-order electron transfer rate in the Asp M184 → Lys mutant argues against the Adir model (*23*) in which the heme edge is docked close to Asp M184. It is likely that that the complex docked in this configuration would exhibit a change in the distance between the heme and the bacteriochlorophyll dimer due the Asp M184 mutation, leading to a change in the first-order rate. Thus, it is more reasonable that the heme edge of the cyt docks at a

Table 2: Ratio of the Binding Free Energy Changes, $\delta\Delta G°$, of Mutant RCs with Charge Changes ($\Delta q = 1$ and 2) at Four Sites on the RC

strain	charge change (Δq)	$\delta\Delta G°$ (meV)	$\frac{\delta\Delta G°(-) \rightarrow (0)}{\delta\Delta G°(-) \rightarrow (+)}$
DN(M184)	1	83 ± 4	0.49
DK(M184)	2	168 ± 5	
DN(M292)	1	42 ± 3	0.47
DK(M292)	2	90 ± 2	
EQ(M95)	1	70 ± 3	0.55
EK(M95)	2	128 ± 4	
DN(L261)	1	39 ± 7	0.30
DK(L261)	2	130 ± 3	

site other than one of the acid residues mutated in this study than to argue (*23*) that the invariance of the first-order rate is the result of a fortuitous cancellation of the effects of mutation.

Strong electrostatic interaction with the M side of the RC around Asp M184 is a feature of all the models for the complex (*17*, *18*, *23*, *25*). Thus, the effects of mutations on binding do not distinguish between the different models. However, recent experiments (*42*), in which the interaction between RCs with acid → Lys mutations and cyt c_2 from *Rhodobacter capsulatus* with complementary Lys → acid mutations was studied, provide additional information about the structure of the complex in solution. The cyt in which Lys 99 (homologous to Lys 103 in *Rb. sphaeroides* cyt c_2) was mutated to Glu had the largest effect in reversing the charge effect on the electron transfer rate k_2 of the Asp M184 → Lys mutation of the RC. This indicates the proximity of Asp M184 and Lys 103 in the cyt c_2:RC complex, in agreement with the Allen model (*17*) and the Axelrod crystal structure (*25*) but not with the Adir (*23*) and Tiede (*18*) models.

Role of Charged Residues in the Binding of the Cytochrome

A number of physical models have been proposed for the nature of the interactions between the charges of the cyt and RC. Early models assumed that salt bridge interactions were necessary to align the two proteins for favorable electron transfer. Attempts at predicting a bound structure involved matching up individual positively charged residues on cyt c_2 with negatively charged residues on the RC to form specific ion pairs after putting constraints on the orientation of the heme (*17*, *18*). These were based on traditional "lock-and-key" models for protein−protein recognition.

Tiede and co-workers proposed a model in which the cyt and RC are brought together by overlapping regions of positive and negative potentials on the two proteins (*13*, *14*). In this model, the electrostatic interactions are more diffuse and do not require specific salt bridges to be formed between charged residues. Evidence for this point of view comes from the observation that a large number of different cyt species can successfully undergo electron transfer with *Rb. sphaeroides* RCs. Although these cyt species have their individual Lys residues at different positions, they all have an area of strong positive potential on the same side of the heme edge. This region was proposed to orient the cyt so that the heme is properly positioned for electron transfer but is not so specific that the individual placement of charges which vary from cyt to cyt is the determining factor in the binding (*14*). Results from our study that have some bearing on the question of the role of charged residues in the formation of an active complex are discussed below.

$\delta\Delta G°$ Due to Mutations of Negatively Charged Residues to Neutral ($\Delta q = 1$) and to Positively Charged Residues ($\Delta q = 2$). The free energy changes obtained by mutating negative Asp or Glu to to their neutral amide forms (charge-neutralizing mutations) compared to the free energy change resulting from mutating the same negative residues to positive Lys residues (charge-reversing mutation) can provide information about the relative contributions of electrostatic, desolvation, and hydrophobic terms to $\delta\Delta G°$ (*32*−*34*). Four sets of mutants were obtained in which acidic residues were replaced with their neutral amides [(−) → (0)] and by positively charged Lys [(−) → (+)]. The ratio of the changes in binding free energy for the charge-neutralizing and charge-reversing mutation, γ, was calculated (see Table 2).

$$\gamma = \frac{\delta\Delta G°(-) \rightarrow (0)}{\delta\Delta G°(-) \rightarrow (+)} \tag{8}$$

In three of the four cases, sites M292, M95, and M184, γ was close to $^1/_2$, as expected from a Coulomb interaction for a charge in a constant potential due to the cyt. For a fourth site, L261, the free energy ratio was approximately $^1/_3$.

Although the ratio of $^1/_2$ is expected from Coulomb's law, the result is somewhat surprising in view of the other factors that may contribute to binding. The ratio γ calculated using the terms in eq 6 is given by

$$\gamma = \frac{e\psi - \Delta G^{DS}}{2e\psi + \delta\Delta G^{HP}} \tag{9}$$

where e is the magnitude of the electron charge. The binding free energy changes in the numerator, due to the acid → amide mutations, are the Coulomb term due to the single charge mutation and the change in desolvation energy due to the change from a charged residue to a neutral species ($\Delta q = 1$). The change in hydrophobic free energy is assumed to be zero for the acid to amide change since this mutation is isosteric. The free energy changes in the denominator, due to the acid to Lys mutations, are the change in Coulomb energy due to the charge reversal ($\Delta q = 2$) and the change in hydrophobic free energy due to the interactions of the larger side chain of Lys. The desolvation term is absent in the denominator since the desolvation energies are the same for the positively and negatively charged residues.

The observed γ value of $^1/_2$ is obtained if the desolvation energy and the hydrophobic term are both small compared to the Coulomb term. An alternative that cannot be ruled out at present is one in which the desolvation term is offset by a favorable hydrophobic binding contribution of the side chains of the Lys. However, a large hydrophobic contribution from Lys seems unlikely due to the polar nature of this residue. Thus, the results suggest that for the charged residues at the three sites, D(M184), D(M292), and E(M95), both the hydrophobic and the desolvation energy changes upon forming the complex are small. The small desolvation energies can be explained if a layer of water molecules

remains between the two proteins upon binding so that the surface charges remain solvated in the complex.

Another requirement for a γ value of $^1/_2$ is that the potential at the native and mutated residues, ψ_i, due to the positive charges on the cyt is the same. Even if it is assumed that the structure of the cyt c_2:RC complex does not change with mutation, the charges on Asp and Lys are unlikely to be located at the same positions within the interface of the complex due to the differences in the length of the Asp and Lys side chains. Thus, this condition requires that the potential surface on the cyt remain approximately constant over a region encompassing the changed position of the side chains. This picture is in accord with the proposal by Tiede et al. (*14*) for electrostatic interaction between diffuse potential surfaces.

$\delta\Delta G°$ of a Double Mutant in Which $\Delta q = 4$. The double mutant DK(L155)/DK(L257) shows a change in free energy of 145 meV. This is close to the sum of the free energy changes for the single mutants (150 meV) and supports the idea that the mutations do not significantly change the structure of the complex.

$\delta\Delta G°$s Due to Mutations of Neutral to Negatively Charged Residues ($\Delta q = -1$). Results from the three mutants that added negative charge on the RC surface support a model in which the charges do not form ion pairs upon binding. These mutations placed negatively charged residues in place of neutral residues on the RC surface ($\Delta q = -1$). Mutants QE(L258), ND(M188), and QE(L264), all on the M subunit side of the periplasmic surface, made the binding energy more favorable by -10, -40, and -85 meV, respectively (see Table 1), resulting in stronger binding mutants. Even though these residues do not form charged pairs with cyt c_2 Lys residues in native RCs, the changes in binding energy are similar in magnitude (i.e., within a factor of 2−3) but opposite in sign to those RC mutants, where negatively charged residues in this region are neutralized ($\Delta q = 1$).

Dynamics of the Association of Cytochrome c_2 and the RC

Relationship between the Second-Order Rate Constant k_2 and the Dissociation Constant K_D. The docking of the cyt onto the RC is an important part of the electron transfer process. The second-order rate constant, k_2, is dominated by the docking dynamics as shown by Allen and co-workers (*43*, *44*), who found that this rate is independent of driving force for electron transfer. In the study presented here, the importance of the association dynamics on the electron transfer rate is shown by the correlation between the second-order rate constant, k_2, and the dissociation constant, K_D (see Figure 6). RCs having the largest K_D have the smallest k_2. For mutants with dissociation constants that are higher than the native value, the data can be fitted to a straight line given by the relationship $\log k_2 = \alpha \log(1/K_D) + \text{constant}$. In the mutant RCs with tighter binding than native, the second-order rate constants do not increase. This may indicate that the diffusion-controlled limit has been reached. The slope of the linear part of the curve (α) was found to be 0.40 ± 0.06 (see Figure 6).

A simple transition state model can be used to explain the correlation between k_2 and K_D. The cyt:RC association starts with an encounter complex, which has nonspecific

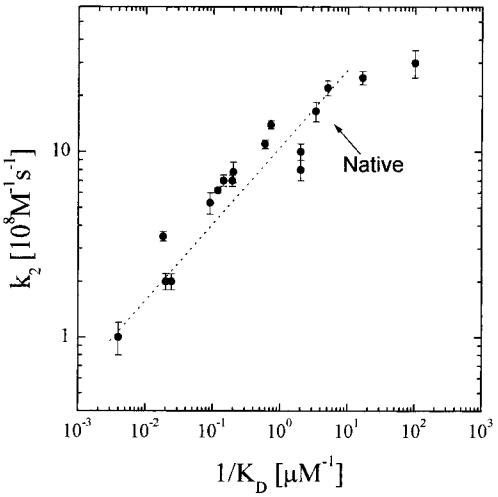

FIGURE 6: Log plot of the second-order rate constant (k_2) vs binding constant ($1/K_D$). The plot shows a correlation between the binding affinity and the rate of collisional electron transfer. The dotted line represents a slope of 0.4, indicating that the transition state resembles both the initial and final states.

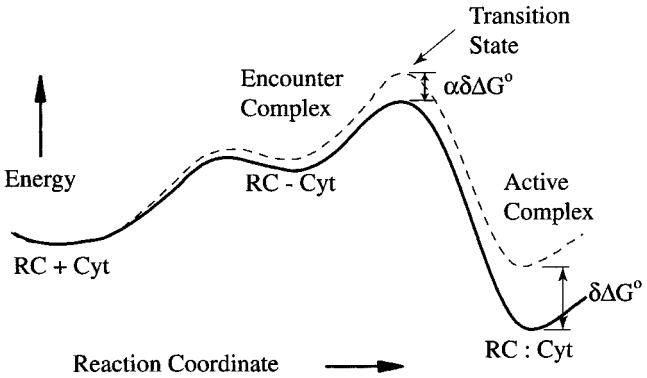

FIGURE 7: Reaction coordinate diagram showing the initial state, the encounter complex, the transition state, and the final active complex for the reaction between cyt c_2 and native (solid line) and mutant (dashed line) RCs. The initial states are arbitrarily set at equal energies. The change in the transition state energy, $\alpha\delta\Delta G°$, is shown as a fraction of the change in the binding free energy, $\delta\Delta G°$, due to mutation. The correlation between log k_2 and log-($1/K_D$) shown in Figure 6 is consistent with an α of 0.4.

electrostatic interactions and fluctuates between configurations in which the intermolecular contacts necessary for electron transfer are not optimized (*46*−*48*) (see Figure 7). The encounter complex can decay by dissociation to the separated RC and cyt or can proceed to the final state via the transition state. The transition state is a specific configuration (or configurations) of the encounter complex, which leads to the final state, optimized for electron transfer.

The reaction coordinate diagram, shown in Figure 7, can account for the dependence of k_2 on binding energy. The effect of a mutation is to change the energy of the final state by $\delta\Delta G°$. The mutation will change the energy of the transition state by some fraction, α, of the binding energy change if a bonding change due to the mutation occurs at the transition state (*45*). The value of α can vary from 0 to 1 depending upon whether the transition state resembles the initial state or the final state. The slope of a logarithmic plot of the rate constant k_2 versus binding constant $1/K_D$ is the average value of α for different mutations. The slope of the plot shown in Figure 6 gives an α value of 0.40, indicating

a transition state that bears a partial similarity to the final state. This is consistent with a transition state in which the cyt and RC are oriented in a manner similar to that of the final cyt:RC complex, except that the distances between charges on the two proteins are longer (by a factor of 2.5, based on a Coulomb interaction and an α of 0.4). We argued previously that the charges in the final complex were well solvated. Thus, if we assume the presence of at least one water molecule in the interface, the closest distance between interacting charges will be in the range of 5−6 Å for the final complex and 12−15 Å for the transition state. The final step would involve movement of the two proteins to form the final complex involved in electron transfer. The rate-limiting step in this process may involve the removal of the solvent from the charged interface. This model for the transition state supports the proposal that long-range electrostatic interactions play an important role in bringing the cyt c_2 into the proper orientation for electron transfer.

The transition state model discussed above is conceptually similar to the three-state model of Moser and Dutton (*11*), which also involves an inactive distal and an active proximal state. However, the details of the inactive distal state are different in the two models because the encounter complex in our model must dissociate rapidly to account for the observed second-order kinetics and the slow transition from the distal to proximal state is not seen in our measurements. The α value of 0.4 is consistent with the treatment used by Gerencsér et al. (*49*) to model their finding of an increased off-rate for cyt with increasing ionic strength. They assumed an electrostatic potential that increased the on-rate and decreased the off-rate equally, as would be the case for an α of $\sim^1/_2$, in approximate agreement with the α value of ≈0.4 found in this work.

Nature of the Cytochrome c_2:RC Complex

Two-Domain Model. The results from this study and the Axelrod crystal structure (*25*) lead us to postulate a two-domain model of the interface region that explains the binding and electron transfer: an electrostatic docking domain that is important for attracting and docking the cyt c_2 to the RC and a hydrophobic tunneling domain that is important for specificity and intimate association of the electron transfer contacts.

The electrostatic docking domain involves negatively charged residues on the RC near Asp M184 interacting with positively charged residues on cyt c_2. The mutational results suggest that the interactions involve well-solvated charges separated by a water layer. The water layer plays an important role in eliminating the energy cost of desolvation of charged groups and in preventing the formation of an excessively strong association between oppositely charged residues. Such a strong association would lead to tighter binding and to a slow dissociation which would be undesirable for the function of the cyt as a reversibly bound electron carrier between the RC and the cytochrome bc_1 complex.

The presence of a hydrophobic tunneling domain is consistent with the finding that mutations of charged residues do not significantly alter the rate constant, k_e, for electron transfer in the bound complex. This shows that the pathway for electron transfer is not changed by these mutations, and suggests that the specificity for docking the heme edge involves a close contact between the heme edge of the cyt and the surface of the RC. An apolar region near Tyr L162 on the RC surface that is located directly over the bacteriochlorophyll dimer provides a surface for such a hydrophobic contact. The interaction of the cyt heme with Tyr L162 has been proposed in several models (*17*, *18*). This interaction is seen in the X-ray structure of the cyt:RC complex from the *Rb. sphaeroides* RC (*25*). The role of Tyr L162 in binding of cyt was demonstrated by the large changes in cyt binding due to mutation of this residue (*50*, *51*). The close contact between the heme and Tyr L162 is advantageous since it avoids the insulating water layer present in the electrostatic docking domain that would reduce the rate of electron transfer.

The mutational results rule out a strict lock-and-key model for the complex based on specific salt bridge interactions in accord with the proposal by Tiede et al. (*14*). However, the two-domain model represents a crude lock-and-key structure for the complex that combines the diffuse electrostatic interaction domain with a hydrophobic domain surrounding the docked heme edge on Tyr L162. The diffuse nature of the interactions in the complex endows the structure with a robustness that has the desirable effect of increasing the probability of forming an active electron transfer state.

SUMMARY

(1) Mutation of acidic residues to Lys on the periplasmic surface of the RC decreases the binding affinity (increases the dissociation constant K_D) for binding of cyt c_2 to the RC. The largest changes occur for mutations to a cluster of residues surrounding Asp M184 asymmetrically located on the M side of the surface. This area is implicated as the region that interacts most strongly with positive residues of the cyt in the RC:cyt c_2 complex.

(2) The mutations that change the binding affinity also change the second-order rate constant, k_2, for electron transfer. The change in k_2 is correlated with the change in K_D, and a plot of log k_2 versus log $1/K_D$ displayed a slope of ∼0.4. The correlation between rate and binding affinity shows that the electrostatic bonding interactions present in the final complex are partially formed in the transition state. This supports the role of electrostatic interactions in orienting the cyt for fast association.

(3) Despite large changes in the binding affinity in these mutant RCs, the first-order rate constant for electron transfer remained unchanged. This rate is due to electron transfer from cyt bound in the cyt:RC complex. The invariance of this rate shows that the distance for electron tunneling is not changed due to the mutation of the charged residues.

(4) The free energy change for the mutation of a negative residue to a neutral residue (removing the electrostatic interaction) was $\sim^1/_2$ of the change of the negative residue to a positive residue (reversing the sign of the electrostatic interaction) for three residues. This ratio of energies suggests that the desolvation energy and hydrophobic energy are small compared to the Coulomb energy and suggests that the charged residues on the RC and cyt are well solvated and do not form salt bridges.

(5) Mutations of neutral residues to negative residues on the RC surface increased the binding affinity of the cyt. The changes in free energy due to these mutations were similar

in magnitude but opposite in sign to changes due to charge-neutralizing mutations in the same general region. This result suggests a diffuse electrostatic potential due to cyt c_2 at the RC surface, consistent with the proposal of Tiede et al. (*14*).

ACKNOWLEDGMENT

We thank Herb Axelrod for discussions of the unpublished work on the X-ray structure of the cyt c_2:RC complex, Andrea Juth, Trieva Turanchick, and Heather Mekosh for technical assistance with the site-directed mutagenesis work, William Parson for assistance in redox potential measurements, John McCoy for assistance in kinetic measurements, Paul Beroza and Arieh Warshel for useful discussions concerning desolvation energy, and Mark Paddock for helpful discussions.

NOTE ADDED IN PROOF

We have postulated in this work the presence of water molecules in the interface between the docked cyt c_2 and the RC. In recent refinements (2.4 Å resolution) of the X-ray structure of the cyt:RC complex, 16 water molecules were resolved in the region of the interface between the cyt and the RC (H. Axelrod et al., unpublished results). This supports the idea of a hydrated interface of the electrostatic docking domain.

REFERENCES

1. Cramer, W. A., and Knaff, D. B. (1990) *Energy Transduction in Biological Membranes*, Springer-Verlag, New York.
2. Margoliash, E., and Brossard, H. R. (1983) *Trends Biochem. Sci. 8*, 316−320.
3. Ferguson-Miller, S., Brautigan, D. L., and Margoliash, E. (1976) *J. Biol. Chem. 251*, 1104−1115.
4. Dutton, P. L., and Prince, R. C. (1978) in *The Photosynthetic Bacteria* (Clayton, R. K., and Sistrom, W. R., Eds.) Chapter 28, Plenum, New York.
5. Feher, G., Allen, J. P., Okamura, M. Y., and Rees, D. C. (1989) *Nature 339*, 111−116.
6. Tiede, D., and Dutton, P. (1993) in *The Photosynthetic Reaction Center* (Deisenhofer, J., and Norris, J., Eds.) pp 258−288, Academic Press, San Diego.
7. Prince, R. C., Cogdell, R. J., and Crofts, A. R. (1974) *Biochim. Biophys. Acta 347*, 1−13.
8. Dutton, P. L., Petty, K. M., Bonner, H. S., and Morse, S. D. (1975) *Biochim. Biophys. Acta 387*, 536−556.
9. Overfield, R. E., Wraight, C. A., and Devault, D. (1979) *FEBS Lett. 105*, 137−142.
10. Rosen, D., Okamura, M. Y., and Feher, G. (1980) *Biochemistry 19*, 5687−5692.
11. Moser, C. C., and Dutton, P. L. (1988) *Biochemistry 27*, 2450−2461.
12. Venturoli, G., Mallardi, A., and Mathis, P. (1993) *Biochemistry 32*, 13245−13253.
13. Tiede, D. M., and Vashista, A.-C. J. (1991) *Mol. Cryst. Liq. Cryst. 184*, 191−200.
14. Tiede, D. M., Vashishta, A. C., and Gunner, M. R. (1993) *Biochemistry 32*, 4515−4531.
15. Larson, J. W., and Wraight, C. A. (2000) *Biochemistry 39*, 14822−14830.
16. Ke, B., Chaney, T. H., and Reed, D. W. (1970) *Biochim. Biophys. Acta 216*, 373−383.
17. Allen, J. P., Feher, G., Yeates, T. O., Komiya, H., and Rees, D. C. (1987) *Proc. Natl. Acad. Sci. U.S.A. 84*, 6162−6166.
18. Tiede, D. M., and Chang, C.-H. (1988) *Isr. J. Chem. 28*, 183−191.
19. Axelrod, H., Feher, G., Allen, J., Chirino, A., Day, M., Hsu, B., and Rees, D. (1994) *Acta Crystallogr. D50*, 596−602.
20. Hall, J., Zha, X. H., Durham, B., O'Brien, P., Vieira, B., Davis, D., Okamura, M., and Millett, F. (1987) *Biochemistry 26*, 4494−4500.
21. Long, J. E., Durham, B., Okamura, M., and Millett, F. (1989) *Biochemistry 28*, 6970−6974.
22. Caffrey, M. S., Bartsch, R. G., and Cusanovich, M. A. (1992) *J. Biol. Chem. 267*, 6317−6321.
23. Adir, N., Axelrod, H., Beroza, P., Isaacson, R. A., Rongey, S. H., Okamura, M. Y., and Feher, G. (1996) *Biochemistry 35*, 2535−2547.
24. Tetreault, M., Rongey, S. H., Feher, G., and Okamura, M. Y. (1997) *Biophys. J. 72*, A7.
25. Axelrod, H. L., Abresch, E. C., Okamura, M. Y., Feher, G., Yeh, A. P., and Rees, D. C. (1999) *Biophys. J. 76*, A20.
26. Rongey, S. H., Paddock, M. L., Feher, G., and Okamura, M. Y. (1993) *Proc. Natl. Acad. Sci. U.S.A. 90*, 1325−1329.
27. Paddock, M. L., McPherson, P. H., Feher, G., and Okamura, M. Y. (1990) *Proc. Natl. Acad. Sci. U.S.A. 87*, 6803−6807.
28. Paddock, M. L., Rongey, S. H., Feher, G., and Okamura, M. Y. (1989) *Proc. Natl. Acad. Sci. U.S.A. 86*, 6602−6606.
29. Simon, R., Proefer, U., and Puhler, A. (1983) *Bio/Technology 1*, 784−791.
30. Brandner, J. P., McEwan, A., Kaplan, S., and Donohue, T. (1989) *J. Bacteriol. 171*, 360−368.
31. Bartsch, R. (1978) in *The Photosynthetic Bacteria* (Clayton, R., and Sistrom, W., Eds.) pp 249−279, Plenum Press, New York.
32. Sharp, K. A., and Honig, B. (1990) *Annu. Rev. Biophys. Biophys. Chem. 19*, 301−332.
33. Warshel, A., and Aqvist, J. (1991) *Annu. Rev. Biophys. Biophys. Chem. 20*, 267−298.
34. Weng, Z., Vajda, S., and DeLisi, C. (1996) *Protein Sci. 5*, 614−626.
35. Kleinfeld, D., Okamura, M. Y., and Feher, G. (1984) *Biochim. Biophys. Acta 766*, 126−140.
36. Nicholls, A., Sharp, K. A., and Honig, B. (1991) *Proteins: Struct., Funct., Genet. 11*, 281−296.
37. Marcus, R. A., and Sutin, N. (1985) *Biochim. Biophys. Acta 811*, 265−322.
38. Venturoli, G., Drepper, F., Williams, J. C., Lin, X., and Mathis, P. (1998) *Biophys. J. 74*, 3226−3240.
39. Moser, C. C., Keske, J. M., Warnke, K., Farid, R. S., and Dutton, P. L. (1992) *Nature 355*, 796−802.
40. Beratan, D. N., Betts, J. N., and Onuchic, J. N. (1991) *Science 252*, 1285−1288.
41. Michel, H., Epp, O., and Deisenhofer, J. (1986) *EMBO J. 5*, 2445−2451.
42. Tetreault, M., Cusanovich, M., Meyer, T., Feher, G., and Okamura, M. Y. (1999) *Biophys. J. 76*, A20.
43. Lin, X., Williams, J. C., Allen, J. P., and Mathis, P. (1994) *Biochemistry 33*, 13517−13523.
44. Wang, S., Li, X., Williams, J. C., Allen, J. P., and Mathis, P. (1994) *Biochemistry 33*, 8306−8312.
45. Page, M., and Williams, A. (1997) *Organic and Bio-organic Mechanisms*, Addison-Wesley, Reading, MA.
46. Koppenol, W. H., and Margoliash, E. (1982) *J. Biol. Chem. 257*, 4426−4437.
47. Northrup, S. H., Boles, J. O., and Reynolds, J. L. (1988) *Science 241*, 67−70.
48. McLendon, G. (1991) *Struct. Bonding 75*, 160−174.
49. Gerencsér, L., Laczkó, G., and Maróti, P. (1999) *Biochemistry 38*, 16866−16875.
50. Farchaus, J., Wachtveitl, J., Mathis, P., and Oesterhelt, D. (1993) *Biochemistry 32*, 10885−10893.
51. Wachtveitl, J., Farchaus, J. W., Mathis, P., and Oesterhelt, D. (1993) *Biochemistry 32*, 10894−10904.

BI010222P